Personal Account

THE CHEMICAL RECORD

doi.org/10.1002/tcr.202300075
tcr.wiley-vch.de

Spectroscopic and Chemical Properties of Ionic Liquids: Computational Study

Hyung J. Kim*[a]

Abstract: A brief account is given of highlights of our computational efforts – often in collaboration with experimental groups – to understand spectroscopic and chemical properties of ionic liquids (ILs). Molecular dynamics, including their inhomogeneous character, responsible for key spectral features observed in dielectric absorption, infra-red (IR) and fluorescence correlation spectroscopy (FCS) measurements are elucidated. Mechanisms of chemical processes involving imidazolium-based ILs are illustrated for CO_2 capture and related reactions, transesterification of cellulose, and Au nanocluster-catalyzed Suzuki cross-coupling reaction with attention paid to differing roles of IL ions. A comparison with experiments is also made.

Keywords: ionic liquids, molecular dynamics, N-heterocyclic carbene, reactions, spectroscopy

1. Introduction

The term "Ionic liquids" designates a diverse class of materials, linked by two criteria: ionicity and liquidity at temperatures, usually below 100 °C. Consisting typically of bulky organic cations paired with weakly basic inorganic or organic anions, ILs possess unique properties, including negligible vapor pressure, high thermal and chemical stability, good ion conductivity, and large electrochemical window. In addition, the tunability of their properties through judicious combinations of countlessly many cations and anions allows for design of task-specific ILs. As such, they afford a wide range of potential applications in many areas of chemistry, electrochemistry, materials science, environmental science, etc.[1–6]

Over the last two decades or so, there has been marked progress in both fundamental understanding and practical applications of ILs, thanks to insightful research contributions by many different groups around the globe.[1–7] Our own effort based on computational approaches, but often in direct collaboration with experimental groups, has been focused on gaining detailed molecular insights into various physicochemical properties of ILs in homogeneous and inhomogeneous environments. Some of our earlier works along this avenue were reviewed previously.[8] In the present account, we give an overview of our more recent contributions, including collaborative works with experimental groups, on two topics – spectroscopy and chemical reactions in ILs. The former include dielectric absorption, IR and FCS with a focus on roles played by individual and collective dynamics of IL ions. For the latter, chemical reactivity/catalytic activity of imidazolium-based ILs is considered briefly for CO_2/COS/CS_2 capture, transesterification of cellulose and alcohols, and gold nanocluster-catalyzed Suzuki cross-coupling reaction. Only main highlights of our results are given here. For details, the reader is referred to original articles.

2. Models and Methods

We begin with a brief description of models and methods employed in our computational studies. For classical molecular dynamics (MD) simulations, all-atom force field parameters, especially those of refs [9]-[11] and OPLS force field,[12] were used for ILs though the CHARMM force field[13] and the

[a] *Prof. H. J. Kim*
Department of Chemistry
Carnegie Mellon University
Pittsburgh, PA 15213, USA
E-mail: hjkim@cmu.edu

coarse-grained model we developed[14] were also employed in some cases. While electronic polarizability is not included in the force field parametrizations we used, they nonetheless provide a computationally efficient description to obtain molecular insights at the semi-quantitative level. This view is corroborated by good agreement with experiments on various IL properties discussed below. Both DL-POLY[15] and GROMACS[16] programs were used for classical simulations. For ab initio MD (AIMD) simulations, the BLYP functional[17] with Grimme's dispersion correction[18] was employed. AIMD simulations were performed using the CP2K program[19] with a time step of 0.5 fs.

3. Dynamics and Spectroscopy

3.1. Dielectric Relaxation of Pure ILs

Fluctuations and relaxation of local electric polarization in the time scale longer than ~0.1 ps occur typically via two different types of motions in ILs: reorientation of ion dipole moments and rearrangement of ion charge distributions through translations.[20,21] As such, dielectric loss, far-IR (FIR) and related tera-Hertz spectroscopies offer an excellent experimental tool to probe these dynamics. The frequency-dependent dielectric constant $\varepsilon(\omega)$ and IR absorption cross section $\alpha(\omega)$ normalized by volume V, both directly accessible via experiments, can be calculated as[22]

$$\varepsilon(\omega) - \varepsilon(\infty) = 4\pi\chi(\omega) = \frac{8\pi^2\beta}{3V}\left\{\langle\vec{M}^2\rangle + iI_{\mathrm{MD}}(\omega)\right\} \tag{1}$$

$$n(\omega)\alpha(\omega) = \frac{8\pi^2\beta\omega^2}{3cV} I_{\mathrm{MD}}(\omega) \tag{2}$$

where ω is the angular frequency, $\chi(\omega)$ is the generalized electric susceptibility, $n(\omega)$ is the index of refraction of the medium, c is the speed of light in vacuum, β is the inverse temperature measured in units of Boltzmann's constant k_B, $\beta = 1/k_BT$, $\vec{M}$ is the system dipole moment, $\langle\cdots\rangle$ is the equilibrium ensemble average and $I_{\mathrm{MD}}(\omega)$ is the lineshape function obtained from MD

$$I_{\mathrm{MD}}(\omega) = \frac{1}{2\pi}\int_{-\infty}^{\infty}\langle\vec{M}(0)\cdot\vec{M}(t)\rangle\exp[i\omega t]\ dt$$
$$= \frac{1}{2\pi\omega^2}\int_{0}^{\infty}\langle\vec{J}(0)\cdot\vec{J}(t)\rangle\ \cos(\omega t)\ dt \tag{3}$$

$$= \frac{1}{2\pi\omega^2}\sum_{\mathrm{A,B}}\int_{0}^{\infty}\langle\vec{J}_{\mathrm{A}}(0)\cdot\vec{J}_{\mathrm{B}}(t)\rangle\ \cos(\omega t)\ dt \tag{4}$$

Here $\vec{J}(t)$ is the time derivative of $\vec{M}(t)$ (i.e., current density integrated over V), and A and B denote ionic/molecular components of the system. Since $\vec{J}$ is well-defined for individual ions while $\vec{M}$ is not, eq 4 provides a convenient framework to analyze IR contributions from different ionic species. Because of non-vanishing dc conductivity σ_{DC} in ionic systems, we also introduce $\varepsilon_c(\omega)$

$$\varepsilon_c(\omega) = \varepsilon(\omega) - i\frac{4\pi}{\omega}\sigma_{\mathrm{DC}} \tag{5}$$

which behaves well (i.e., non-singular) at $\omega = 0$.

The results for EmimETS (1-ethyl-3-methylimidazolium ethyl sulfate) obtained via classical MD are presented in Figure 1.[23] The imaginary part of $\varepsilon_c(\omega)$ shown in red exhibits a conspicuous peak near $\omega = 0.001$ ps^{-1} in Figure 1a. Though not presented here, analysis by decomposing $\vec{M}(t)$ into contributions from center-of-mass translational motions and rovibrational motions of ions indicates that this absorption band arises primarily from reorientational dynamics, in particular diffusive rotations, of ETS^-. The contribution of cations is considerably smaller than that of anions because the center-of-mass dipole moment of $Emim^+$ is smaller and thus their reorientations modulate $\vec{M}(t)$ much less than ETS^-. We notice that $\varepsilon_c(\omega)$ shows dielectric absorption also in the THz region, i.e., ω ~0.1–20 ps^{-1}. This is mainly due to translational motions of ions though hindered rotations (i.e., librations) of anions also make a non-vanishing contribution (see Figure 2 below). For a better exposition, the contribution to $\varepsilon_c(\omega)$ arising from center-of-mass translational motions of cations and anions, $\varepsilon_{\mathrm{tr}}^{\mathrm{cm}}(\omega)$, is displayed in Figure 1b. It shows a

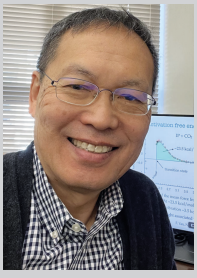

Hyung Kim received his PhD in Chemical Physics from the State University of New York at Stony Brook in 1988, working with the late Prof. Harold L. Friedman. After postdoctoral research in Chemistry at the University of Colorado, Boulder, under the supervision of Prof. James T. Hynes, he joined the faculty of Carnegie Mellon University in 1992 and is currently Professor of Chemistry there. The main theme of his research is theoretical understanding of chemical processes and closely related spectroscopy in homogeneous and heterogeneous environments. By employing electronic structure theory and simulation methods as well as theoretical modeling, he studies free energetics, dynamics and mechanisms of reactive and non-reactive processes in solutions and at solid-liquid interfaces and their spectroscopic properties.

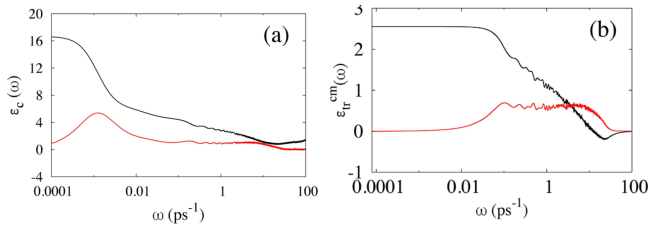

Figure 1. Classical MD results for (a) fequency-depedent dielectric constant $\varepsilon_c(\omega)$ and (b) its translational component $\varepsilon_{tr}^{cm}(\omega)$ for EmimETS at 350 K. $\varepsilon_{tr}^{cm}(\omega)$ is calculated by considering only the ion center-of-mass translational motions in eqs 1 and 4. The real and imaginary parts of the dielectric constants are shown in black and red lines, respectively. Reprinted with permission from ref. [23] (Copyright 2017 American Chemical Society).

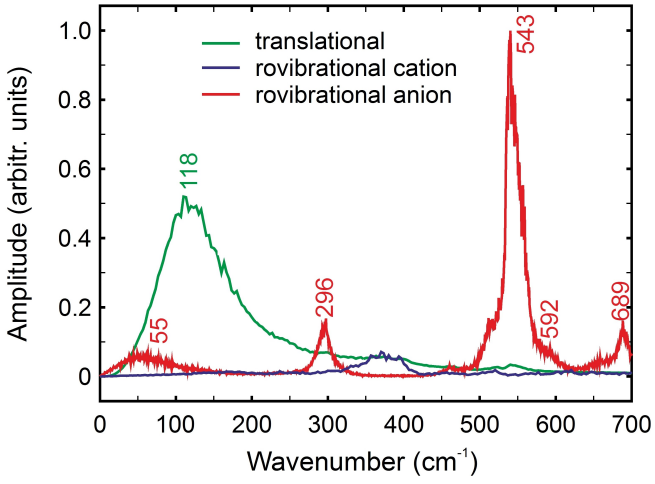

Figure 2. Classical MD results for translational and rovibrational components of the far-IR spectrum of EmimETS at 350 K. Reprinted with permission from ref. [23] (Copyright 2017 American Chemical Society).

transition from the anomalous to normal dispersion near $\omega = 20$ ps^{-1}, revealing that the absorption mode there has a resonance character. This is attributed to the hindered oscillation character of ion translations. The broad and multi-peak nature of the THz band suggests that there is at least one more mode near $\omega = 0.3$ ps^{-1}. This sub-terahertz mode is ascribed to dissipative relaxation of ion translations. Another interesting aspect of $\varepsilon_{tr}^{cm}(\omega)$ is that its real part (black line) does not vanish as $\omega \to 0$. This means that the translational motions of ions make a small but important contribution to the static dielectric constant $\varepsilon_c(0)$.

For additional insight, MD results for translational and rovibrational components of the FIR spectrum of EmimETS are presented in Figure 2. The main FIR feature corresponding to the THz band of $\varepsilon_c(\omega)$ in Figure 1b is the broad absorption structure centered at 118 cm^{-1} (green) arising from hindered translations of ions. This band is characteristic of ILs and well-studied in the literature.[24,25] Though not shown here, we mention that collective translational motions of anions and of cations are fully correlated in pure IL systems.[23] The presence of an anion peak at 55 cm^{-1} (red) provides direct evidence that hindered rotations of ETS^- also make a non-negligible contribution to the THz band as noted above. Other anion peaks at 296 cm^{-1} and 543 cm^{-1} are assigned to various ethyl group vibrations and SO_3 wag. MD shows a very reasonable agreement with experimental FIR results[24a,b] with peaks at 106 and 245 cm^{-1} and a minor structure around 50 cm^{-1}

We have also investigated T-dependence of dielectric relaxation.[21b] The MD results for 1-butyl-3-methylimidazolium hexafluorophosphate ($BmimPF_6$) are shown in Figure 3. In contrast to the EmimETS case above, reorientational motions of PF_6^- do not contribute to dielectric relaxation because of its near spherical symmetry. Therefore the rotational component $\varepsilon_{rot}^{cm}(\omega)$ of $\varepsilon_c(\omega)$ in Figure 3a derives exclusively from $Bmim^+$ reorientations. Despite this difference, dielectric relaxation of $BmimPF_6$ occurs mainly via ion reorientations in the GHz region (Figure 3a) and ion translations in the THz region (Figure 3b) just like EmimETS in Figure 1. As T increases, relaxation in the GHz region becomes faster whereas that in the THz region remains largely unaffected. The former is due to the acceleration of rotational diffusion of Bmm^+ with T. The latter on the other hand is ascribed to the weak T-dependence of the effective potential energy surface, upon which ion translational dynamics occur. Structural analysis based on radial distribution functions (not shown here) confirms this.[21b] These differing T-behaviors of relaxation dynamics in the GHz and THz regions are in excellent agreement with experimental results though IL systems studied are different.[26] Another prominent feature of Figure 3 is that as T rises, the translational and reorientational contributions, $\varepsilon_{tr}^{cm}(0)$ and $\varepsilon_{rot}^{cm}(0)$, to the static dielectric constant $\varepsilon_c(0)$ increases and decreases, respectively. These antagonistic roles of $\varepsilon_{tr}^{cm}(0)$ and $\varepsilon_{rot}^{cm}(0)$ explain why the T-dependence of $\varepsilon_c(0)$ of ILs is considerably weaker than that of normal polar solvents, in which only reorientational dynamics contribute to $\varepsilon_c(0)$.

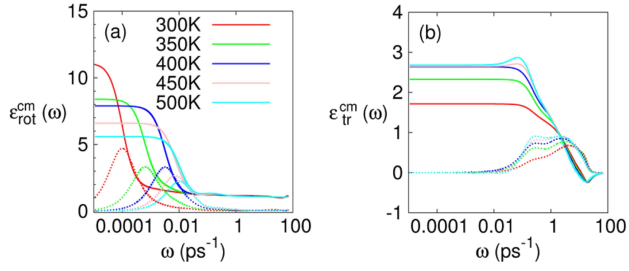

Figure 3. Classical MD results for contributions of (a) reorientational and (b) translational dynamics to $\varepsilon_c(\omega)$ for $BmimPF_6$. The real and imaginary parts of $\varepsilon_c(\omega)$ are plotted as solid and dotted lines, respectively. Reprinted with permission from ref. [21b] (Copyright 2013 American Chemical Society).

We note that while details may differ, several key features of $\varepsilon_c(\omega)$ above are shared by many ILs. These include dielectric relaxation via ion reorientations in the GHz region, ion translations in the THz region and their differing behaviors with temperature. Another is the weak T-dependence of the static dielectric constant of ILs, arising from the antagonistic roles played by $\varepsilon_{tr}^{cm}(0)$ and $\varepsilon_{rot}^{cm}(0)$ as T rises.

3.2. IR Spectroscopy of Pure and Li-Containing ILs

We turn to IR properties of ILs, especially, their changes with the addition of Li salts. While IR spectroscopy of pure ILs has attracted a great deal of interest,[27] IL solutions of Li salts have not received much attention.[28,29] The AIMD results for pure $EmimBF_4$ (1-ethyl-3-methylimidazolium tetrafluoroborate) and its mixture with $LiBF_4$ in the far-IR region are compared with experimental results in Figure 4.[30] The peaks labeled as sa# and sc# (e.g., sa2 and sc10) in the simulated spectra are related to vibrational modes a# (anion) and c# (cation), respectively (see below). Simulation and experiment show good overall agreement though the former results are generally red-shifted by $\lesssim 50\ cm^{-1}$ compared to the latter for $\bar{\nu} \gtrsim 200\ cm^{-1}$. The most salient feature is that the IR absorption in the $250\ cm^{-1} \lesssim \bar{\nu} \lesssim 500\ cm^{-1}$ region increases rapidly with the Li^+ mole fraction, x_{LiBF_4}. Similar spectral changes with dissolution of Li^+ ions were also observed in organic solvents.[31–33] Another noticeable change is the development of a shoulder structure around $550\ cm^{-1}$ ($521\ cm^{-1}$ in AIMD) with increasing x_{LiBF_4}. These features are associated with hindered translational motions ("rattling") of Li^+ ions in differing solvation environments.[31–33] Analysis via eq 4 shows that autocorrelation of Li^+ current, $\vec{J}_{Li}$, is the primary contributor to the FIR band between 250 and $450\ cm^{-1}$ (Figure 4c). Inspection of Li^+ solvation structure (not presented here) indicates that Li^+ rattles (i.e., vibrates) in a cage formed by four BF_4^- anions. We note that cross correlations of Li^+ and IL ion currents make a considerable contribution to this band, revealing that correlated motions of $Emim^+ + Li^+$ and $BF_4^- + Li^+$ are also involved (Figure 4d). Based on these results, we conclude that in the Li^+-rattling band, intramolecular vibrations of ions in and near the Li^+ coordination shell, as well as vibrations of the coordination shell itself, are all coupled to Li^+ motions. Its broad nature derives from differing Li^+ solvation environments that yield a distribution of Li^+ vibrational frequencies. The shoulder structure at $548\ cm^{-1}$ is attributed to Li^+ vibrations combined with hindered translations and antisymmetric bending (a2 in Figure 4e) of BF_4^-.

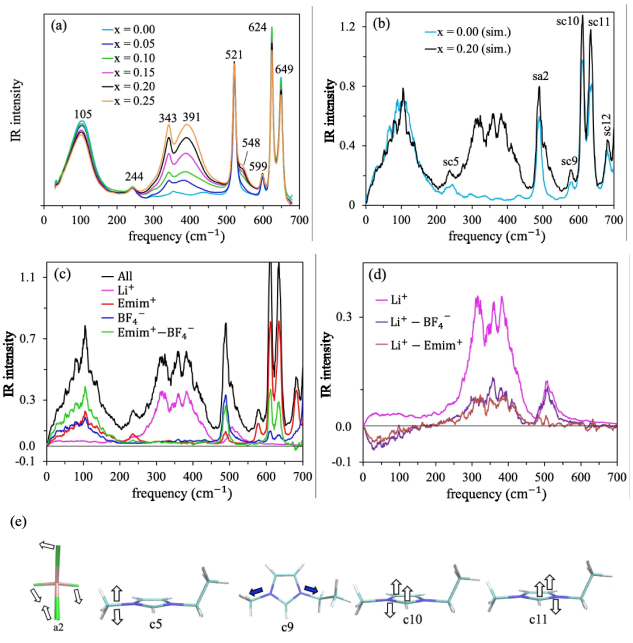

Figure 4. Far-IR spectra of pure $EmimBF_4$ and the $EmimBF_4 + LiBF_4$ mixtures: (a) Experimental results; (b) AIMD results ($n(\omega)\alpha(\omega)$, eq 2; units: $10^3\ cm^{-1}$); (c), (d) decomposition of the AIMD spectrum (eq 4); (e) generalized normal modes. Results in (c) and (d) are for the mixture at $x_{LiBF_4} = 0.2$. In (e), arrows represent directions of vibrations. The filled arrows denote motions along a bond direction, while motions in other directions, such as bending, are displayed in open arrows. Only large-amplitude motions are shown. AIMD peak sc12 in (b) corresponds to the $701\ cm^{-1}$ peak observed in experiment in Figure 5a. Reprinted with permission from ref. [30] (Copyright 2022 American Chemical Society).

Other spectral features in the FIR region, including the broad band around $100\ cm^{-1}$ and the peaks at 244, 521, 599, 624 and 649 cm^{-1} (sc5, sa2, sc9, sc10 and sc11 in AIMD), are not affected significantly by Li^+. This implies that these peaks arise mainly from vibrations of IL ions. Generalized normal modes (GNMs)[34] of ions largely responsible for these peaks are shown in Figure 4e, though other GNMs not shown there may also contribute by coupling to these modes. Qualitatively speaking, GNMs are the average intramolecular vibrations of single ions around their reference structures, corresponding to minima on the potential energy surface of the isolated ion.[34] As in the case of EmimETS above, the broad band around $100\ cm^{-1}$ is assigned to hindered translations of $Emim^+$ and BF_4^-.[21a] Interestingly, the contributions to this band from $Emim^+$-Li^+ and BF_4^- - Li^+ cross correlations are negative for $\bar{\nu} \lesssim 120\ cm^{-1}$ in the mixture (Figure 4d). This indicates that $\vec{J}_{Li}$ is anti-correlated with IL cation and anion currents, $\vec{J}_{Emim}$ and $\vec{J}_{BF_4}$; i.e., they are of opposite directions. This means that Li^+ and its solvation cage consisting of BF_4^- generally translate together in the timeframe corresponding to this frequency range, i.e., $t \gtrsim 250$ fs. This is in general agreement with a recent MD result that Li^+-containing clusters carry a negative charge in ILs.[35]

IR spectra in the fingerprint region are exhibited in Figure 5. Except for the intense band near 1000 cm^{-1}, the addition of $LiBF_4$ does not introduce any major spectral changes, implying limited influence of Li^+. In fact, the contributions from time correlation functions involving $\vec{J}_{Li}$ (not shown here) are totally negligible throughout this region, indicating that Li^+ dynamics do not play any role in the mid-IR spectrum. The pronounced absorption band around 1000 cm^{-1} in the experimental spectrum (Figure 5a) arises mainly from antisymmetric B–F stretching vibrations a4 of BF_4^- (Figure 5c). In pure $EmimBF_4$, this band is characterized by a single primary peak with substructure, in good agreement with a previous IR study.[36] In the mixture, it broadens and develops a double-peak structure with several minor peaks/shoulders. These spectral changes, reproduced reasonably well in the AIMD band sa4 (Figure 5b), are due to Li^+-induced changes in the solvation of BF_4^-. Strong coordination of Li^+ by F of BF_4^- makes local environments of these anions structurally much more diverse and thus the distribution of their stretching frequencies significantly broader in the mixture than in pure $EmimBF_4$. The new peak at 978 cm^{-1} (887 cm^{-1} in AIMD) is assigned to B–F stretching vibrations of F atoms that coordinate to Li^+, while other structures of the band (as well as corresponding structures in neat IL) are attributed to those of non-coordinating F, subject to differing solvation environments, including coupling with $Emim^+$ vibrations.

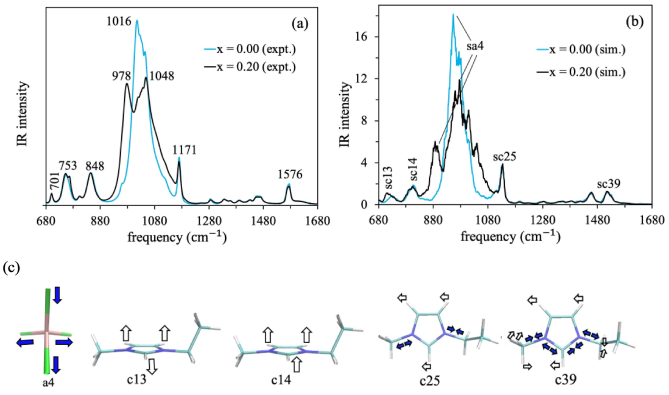

Figure 5. Mid-IR spectra of pure $EmimBF_4$ and the $EmimBF_4 + LiBF_4$ mixture ($x_{LiBF_4} = 0.2$) in the fingerprint region: (a) Experimental results; (b) AIMD results ($n(\omega)\alpha(\omega)$, eq 2; units: 10^3 cm^{-1}); (c) generalized normal modes. Reprinted with permission from ref. [30] (Copyright 2022 American Chemical Society).

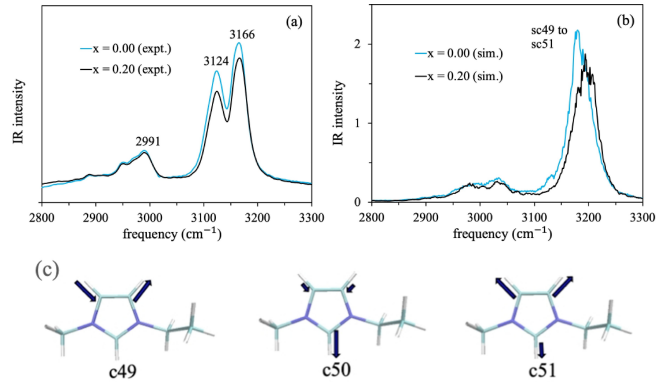

Figure 6. Mid-IR spectra of pure $EmimBF_4$ and the $EmimBF_4 + LiBF_4$ mixture in the C–H stretching region: (a) Experimental results; (b) AIMD results ($n(\omega)\alpha(\omega)$, eq 2; units: 10^3 cm^{-1}); (c) generalized normal modes for C–H stretching vibrations of the $Emim^+$ ring. Reprinted with permission from ref. [30] (Copyright 2022 American Chemical Society).

IR results for the CH stretching region, 2800–3300 cm^{-1}, are displayed in Figure 6. Analogous to neat imidazolium ILs studied extensively,[37–41] the highest-frequency bands in this region arise from C–H stretching vibrations of the $Emim^+$ ring (c49–c51 in Figure 6c). The two distinct peaks at 3124 cm^{-1} and 3166 cm^{-1} in the experimental spectrum are realized as a peak-shoulder structure in AIMD. A detailed analysis indicates that BF_4^- makes a significant contribution to the 3150–3250 cm^{-1} region through cross correlation with $Emim^+$ even though no vibrations are available for BF_4^- at such a high frequency. This is an example of the interaction-induced effect on IR absorption. Weak hydrogen bonds between F of BF_4^- and acidic H of the $Emim^+$ ring modulate the electronic charge distribution of BF_4^- at C–H vibration frequencies, thereby increasing the intensity of the band. By contrast, IR band around 3000 cm^{-1}, resulting from C–H stretching vibrations of the $Emim^+$ alkyl groups, does not show any interaction-induced contributions according to our analysis. This is an electronic manifestation of the absence of any significant interactions between "nonpolar" $Emim^+$ alkyl groups and "polar" BF_4^- anions, well appreciated from the perspective of heterogeneous IL structures.[42] The calculated frequencies of the C–H stretches are higher than their experimental counterparts by $\lesssim$90 cm^{-1}, in contrast to most other IR peaks whose calculated frequencies are lower than those observed. Aside from the exact locations and detailed structures of IR peaks, the AIMD simulations yield good overall agreement with experiment in the CH stretching region.

3.3. Fluorescence Correlation Spectroscopy and Dynamic Heterogeneity of ILs

Polar and nonpolar groups of ILs form nanostructured regions of distinct polarities and their domain size depends on the alkyl chain length of ILs.[42] One of the methods to probe local heterogeneity in ILs is fluorescence correlation spectroscopy (FCS), which reports on the translational dynamics of fluorescent dyes at low concentration. In prior FCS studies, apparent bimodal diffusion observed in ILs was ascribed to

transport of the dyes in the polar versus nonpolar regions.[43,44] However, this interpretation is questionable because it would imply that the probe molecules do not switch between different polarity regions while passing through the FCS focal volume, a process that takes milliseconds.

To shed light on the issue of bimodal diffusion, we have investigated dynamic heterogeneity of ILs with a combined method of FCS and MD.[45] While many experimental[46–53] and computational[21,54–60] studies have revealed an array of interesting features indicative of heterogenous dynamics in ILs, our main focus was the possibility of a correlation between the diffusion of a solvatochromic dye and local polarity of its environment, or lack thereof. Nile Red (NR) was employed as the probe in FCS experiment. As NR has a strong positive solvatochromism, its translational motion in regions of differing polarities can be followed by the photocurrent correlation function $G(t)$ at the red edge and the blue edge of its emission spectrum. Measured $G(t)$ is directly related to the self-van Hove function $G_s(\vec{r}-\vec{r}';t)$ of the dye[61]

$$\begin{aligned} G(t) &\propto A(\lambda)\int d^3r\int d^3r'\int d^2\Omega \\ &\int d^2\Omega' P(\vec{r})P(\vec{r}')\,G_s(\vec{r}-\vec{r}';t); \\ G_s(\vec{r}-\vec{r}';t) &= \sum_i \langle \delta(\vec{r}-\vec{r}_i(t))\delta(\vec{r}'-\vec{r}_i(0))\rangle \end{aligned} \tag{6}$$

where $A(\lambda)$ is the detector-related factor (λ = wavelength), $P(\vec{r})$ is the laser profile, $d^2\Omega$ is the integration over the collection solid angle, $\vec{r}_i(t)$ is the position of the dye molecule i at time t, and the sum is over all dye molecules. In eq 6, it is assumed that the dye is the only molecular species that interacts with light and neither the excitation nor the emission is polarized.

Results for $G(t)$ in the ionic liquid, 1-methyl-1-butylpyrrolidinum bis(trifluoromethylsulfonyl)imide ($Pyrr_{14}Tf_2N$), are shown in Figure 7a. Three different combinations of long pass (LP), short pass (SP) and band pass (BP) filters were used to measure $G(t)$ at the red edge and blue edge of the NR emission spectrum, which ranges from ~550 to ~750 nm in $Pyrr_{14}Tf_2N$. Though there is some variance, the results for the red edge (polar IL region) and the blue edge (nonpolar IL region) are similar within any given set of filters; they all show a significant departure from a unimodal diffusion. This implies that solute diffusion does not vary with local polarity, i.e., translational dynamics of the probe are not correlated with the polarity of its local environment.

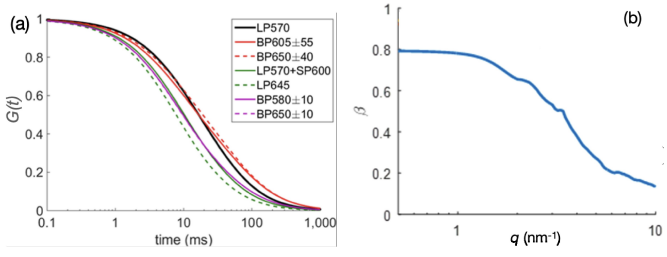

Figure 7. (a) Normalized and fitted $G(t)$ of NR in $Pyrr_{14}Tf_2N$ with various filter sets and (b) the stretched exponential as a function of q for $F_s(q,t)$ for C153 in HmimPF6. In (a), the numbers in the legend denote the range of the wavelength (nm) of the filters used. Reprinted with permission from ref. [45] (Copyright 2017 American Chemical Society).

For further insight, we have investigated $G_s(\vec{r}-\vec{r}';t)$ and its Fourier transform $F_s(\vec{q},t)$ (intermediate self-van Hove function) of model coumarin 153 (C153) in $HmimPF_6$ (Hmim = 1-hexyl-3-methylimidazolium) via MD.[45] The results for $F_s(\vec{q},t)$ exhibit non-exponential relaxation, indicating anomalous diffusion of C153. Fitting these results to a stretched exponential function, $\exp\left[-(t/\tau_\beta)^\beta\right]$, yields the β value, which is less than unity at all q and plateaus to ~0.8 for $q \lesssim 1\ \mathrm{nm}^{-1}$ (Figure 7b). In the $q \to 0$ limit relevant for FCS experiment due to its large length scale ($\gg$1 nm), $G(t)$ can be approximated as[62]

$$\frac{G(t)}{G(0)} = \frac{[1+\xi^2]^{1/2}}{\left[1+\left(\frac{t}{\tau_0}\right)^\beta\right]\left[1+\xi^2\left(\frac{t}{\tau_0}\right)^\beta\right]^{1/2}} \tag{7}$$

where ξ characterizes the focal volume, i.e., the ratio of its axial and radial dimensions. Equation 7 with $\beta \approx 0.8$ and $\tau_0 \approx$15–30 ms well describes FCS results for NR in different ILs we studied.[45] This finding, combined with the FCS results and timescale noted above, strongly indicates that the anomalous diffusion and related dynamic heterogeneity provide a more sensible picture for dye transport in ILs than the bimodal diffusion.

We have also studied glassy behaviors and dynamic heterogeneity of pure ILs via MD.[14b] Analysis of $EmimPF_6$ using a coarse-grained model description shows the breakdown of the Stokes-Einstein relation, indicating it is a fragile glass former. This implies that diffusion of IL ions is enhanced compared to structural relaxation measured by the intermediate van Hove function. Another noteworthy result is that compared with non-ionic models of supercooled liquids,[63] glassy dynamics of $EmimPF_6$ occur at a considerably high temperature. Analysis of instantaneous power inputs to ions arising from Lennard-Jones (LJ) and Coulomb interactions reveals that they are anticorrelated and their time integration, viz., energy input that drives ion translations, is dominated by the LJ interactions. This is also the case with vibrational energy relaxation in ILs.[64] These results indicate that relaxation dynamics of ILs are dominated by the LJ interactions, while the Coulomb interactions exert a strong influence on the liquid structure and thus set the energy and therefore temper-

ature scale for glassy dynamics. This also explains why dynamic aspects of glassy ILs are very similar to those of non-ionic supercooled liquids.

To understand the dynamic behavior of structurally correlated ions, we have investigated a time-dependent 4-point density correlation function[65–69]

$$g_4^{ol}(\vec{r},t) = \frac{V}{N_A N_B} \left\langle \sum_{ij\in A}\sum_{kl\in B} \delta(\vec{r}-\vec{r}_k(0)+\vec{r}_i(0)) \; w\big(|\vec{r}_i(0)-\vec{r}_j(t)|\big)\, w(|\vec{r}_k(0)-\vec{r}_l(t)|) \right\rangle \quad (8)$$

for two different ILs, ChoAc (Cho = choline; Ac = acetate) and BmimAc.[70] In eq 8, i, j, k and l denote individual ions, and $w(r)$ is a coarse-graining function[66c] introduced to remove the effect of local vibrations. $g_4^{ol}(\vec{r}, t)$ – a direct extension of the full van Hove function – describes the time evolution of correlation of density fluctuations occurring simultaneously at two different positions, separated by $\vec{r}$. As such, it gauges the four-particle conditional probability, viz., given a particle of species A at position 1 and a particle of species B at position 2 at the initial time $t=0$, it measures (up to a constant) the probability that the same or another particle of A and the same or another particle of B will be found at positions very close to the original locations 1 and 2, respectively, at a later time. Analysis via MD shows that dynamic correlation between ions beyond their first ionic solvation shell persists longer than 10 ns for both ChoAc and BmimAc at 350 K.[70] By contrast, the time and length scales of dynamic correlation for the normal solvent acetonitrile are, respectively, very short (~1 ps) and smaller than its molecular size at 300 K. This reveals the cooperative nature of ion motions in ILs. The deviation of IL transport from Gaussian dynamics is often measured by[55,57a,58,69]

$$a_2(t) = \frac{3}{5}\frac{\langle \Delta r^4(t)\rangle}{\langle \Delta r^2(t)\rangle^2} - 1 \quad (9)$$

where $\Delta r(t)$ is the displacement of ions at t from their initial positions. (For a Gaussian process, $\alpha_2(t) = 0$.) It was found that $\alpha_2(t)$ and the susceptibility $\chi_4(t)$ associated with $g_4^{ol}(\vec{r}, t)$ exhibits very similar temporal behaviors for both ILs.[70] This implies that the non-Gaussian behavior of individual ions is directly linked to time-dependent correlated motions of ions, i. e., cooperative dynamics.

4. Chemical Reactions in Imidazolium-Based Ionic Liquids

Ionic liquids, in particular imidazolium-based ILs, play many different roles in chemical reactions. In addition to serving as solvent media, they can act as a reaction partner, as a catalyst or as an activator of catalysts. In the remainder of this account, we present highlights of our work on these topics.

4.1. CO_2 Capture in Imidazolium Acetate

Mechanisms of various reactions in the imidazolium acetate IL family, such as trapping reactions,[71] benzoin condensation,[72–75] CO_2 capture,[76–80] etc., have been the subject of much controversy. This is largely due to differing and confusing views on N-heterocyclic carbene (NHC) (Figure 8a), viz., whether it would be formed in neat imidazolium acetate ILs and what roles it would play if indeed formed. Despite the lack of direct experimental evidence, it has been generally believed that NHC is produced via transfer of acidic proton (denoted as H2 hereafter) of imidazolium to one of the oxygen atoms of weakly basic acetate (Figure 8b). NHC thus formed is assumed to play an active role in most of the aforementioned reactions in this IL family ("carbene mechanism").

For insight into the formation of NHC, we have performed ab initio calculations for the ion pair composed of $Emim^+$ and Ac^- ions and the corresponding neutral pair consisting of NHC and acetic acid (Figure 8b) using the SCRF (self-consistent reaction field theory) method.[81] The results strongly suggest that the carbene formation in Figure 8b is highly unlikely, especially in a polar environment, such as ILs. Due to the solute-solvent Coulomb interactions, the ion pair state is stabilized in solution, compared to neutral pair. Our analysis predicts that when the solvent dielectric constant exceeds ~5, the neutral pair state becomes unstable. This means that NHC would not be formed in neat imidazolium acetate, calling into question the carbene mechanism often invoked for many different reactions in this IL family.

Using constrained AIMD, we examined CO_2 capture in EmimAc.[81] The distance between the C atom of the CO_2 molecule that is being captured and the C2 site of $Emim^+$ (C2 = carbon atom H2 is bonded to, Figure 8b) was employed as the reaction coordinate. We found that (successful) H2

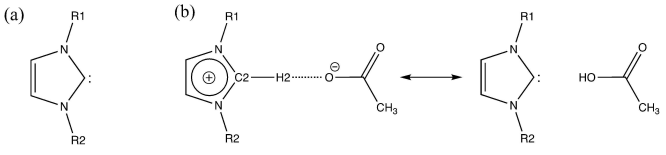

Figure 8. (a) N-heterocyclic carbene (NHC) and (b) putative NHC formation in imidazolium acetate ILs.

transfer occurs only when the CO_2 molecule approaches within ~2.1 Å of the C2 site of $Emim^+$. Snapshots of a successful H2 transfer event are displayed in Figure 9. Furthermore, removal of the constraint on the C2-CO_2 distance upon H2 transfer results in the rapid formation of 1-ethyl-3-methylimidazole-2-carboxylate (Emim-CO_2) in ~30 fs. These findings suggest that CO_2 capture in EmimAc occurs in a concerted fashion, viz., simultaneous H2 transfer and carboxylate formation, and that carbene is not involved. We thus proposed a novel concerted mechanism for CO_2 capture in imidazolium acetate:[81]

$$Emim^+ + Ac^- \underset{k_b}{\overset{k_f}{\rightleftharpoons}} IP \quad \text{(i)}$$

$$IP + CO_2 \underset{k_d}{\overset{k_a}{\rightleftharpoons}} T^{\ddagger} \quad \text{(ii)}$$

$$T^{\ddagger} \xrightarrow{k_c} P \quad \text{(iii)}$$

where IP, $T^{\ddagger}$ and P represent the hydrogen-bonded $Emim^+ \cdots Ac^-$ ion pair, activated termolecular complex (e.g., Figure 9a) and product, respectively, and k_f, k_b, k_a, k_d and k_c are the rate constants for the steps they are associated with. Both classical and ab initio MD predict that virtually all $Emim^+$ and Ac^- ions exist as ion pairs, most of which form a hydrogen bond between H2 of $Emim^+$ and O of Ac^- in the IL phase. Since the formation of $T^{\ddagger}$ is slow (see below), step (i) is likely to be at equilibrium ("pre-equilibrium"). The product formation rate then becomes

$$\frac{d[P]}{dt} = \kappa\, k_a\, [IP][CO_2]\,; \quad \kappa = \frac{k_c}{k_c + k_d}\ (< 1) \quad (10)$$

where [A] denotes the concentration of A. As κ is expected to be comparable to 1, the formation of $T^{\ddagger}$, i.e., CO_2 approach to $Emim^+$, hydrogen-bonded to Ac^-, is rate-limiting. The activation barrier for this step was estimated to be ~19–20 kcal/mol. The concerted mechanism predicts that the reaction is apparently of first order in CO_2 concentration. This is consistent with the experimental observation that increasing the CO_2 pressure accelerates CO_2 chemisorption.[77]

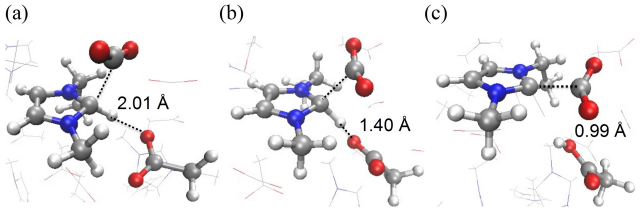

Figure 9. Snapshots of proton transfer from $Emim^+$ to Ac^-. The distance between C2 and C of CO_2 was fixed at 2.1 Å during the simulation and the distance between transferring H2 and accepting O is given in each snapshot. As shown in (c), the product compound Emim-CO_2 is nearly formed as H2 transfer is completed. Reproduced from ref. [81] with permission from the Royal Society of Chemistry.

4.2. Reactions of CS_2 in Imidazolium Acetate

It was observed experimentally that a mixture of CS_2 with BmimAc produces 1-butyl-3-methylimidazole-2-thiocarboxylate and -2-carboxylate, Bmim-COS and Bmim-CO_2, but not 1-butyl-3-methylimidazole-2-dithiocarboxylate, Bmim-CS_2, even though COS and CO_2 were completely absent in the reaction system initially.[82a,b] Based on ab initio calculations in the gas phase, this interesting result was attributed to S/O exchange with Ac^-, which converts CS_2 to COS and some of COS thus produced to CO_2, prior to the capture reaction.[82b,c] Motivated by this work, we performed ab initio SCRF calculations and AIMD simulations to obtain molecular details for solution-phase reactions of CS_2 in imidazolium acetate and to gain further insight into issues surrounding NHC in this IL family.[83]

We have obtained several important results: First, the activation free energy for CS_2 capture by EmimAc is much higher than that for its conversion to COS via S/O exchange. As such, reactions involving CS_2 proceed almost exclusively along the conversion pathway. Second, the activation barrier heights for COS capture and its conversion to CO_2 are comparable. Therefore, some of COS reacts with EmimAc and produces Emim-COS, while some of it further converts to CO_2, which is then captured by EmimAc and generates Emim-CO_2. These results are in perfect agreement with experiments.[82a,b] Additionally, we have investigated CS_2 reaction pathways in the presence of NHC in the reaction system. The free energy barrier for CS_2 capture by NHC was found to be considerably lower than that for CS_2 conversion to COS. This means that if NHC is indeed present in the imidazolium acetate ILs, it will react with CS_2 and produce 1-ethyl-3-methylimidazole-2-dithiocarboxylate, Emim-CS_2, prior to the CS_2-to-COS conversion. This finding, combined with the absence of the imidazole-2-dithiocarboxylate compound in real reaction systems,[82a,b] lends strong support to our view above that NHC is not formed in the imidazalium acetate ionic liquids.[81] One notable consequence of our analysis is that if the formation of NHC can be induced in imidazolium acetate, e.g., by the addition of a strong base, imidazole-2-dithiocarboxylate species would be generated as the product of the capture of CS_2. It would thus be interesting to check if this prediction will be borne out experimentally. This will not only provide additional insight into the CS_2 reaction mechanisms in imidazolium acetate but also cast illuminating light on the controversial NHC formation in this IL family.

4.3. IL-Catalyzed Transesterification of Cellulose

Since the discovery of dissolution of cellulose in ILs,[84] biomass processing and engineering has emerged as one of the important areas of IL applications.[85–88] One example is cellulose modification via EmimAc-catalyzed transesterification with isopropenyl acetate (IPA) as an ester donor.[89,90] To understand the catalytic mechanism of this process, we performed ab initio calculations using methanol (MeOH) as a model for hydroxyl groups of cellulose.[90] The results indicate that it is not $Emim^+$ but Ac^- that catalyzes the transesterification reaction. Acetate interacts strongly with the hydroxyl hydrogen of MeOH, resulting in a significant elongation of its O–H bond. This increases the magnitude of the partial charge of methanol oxygen and thus "activates" it to react with carbonyl group of the ester (Scheme 1).

Additional mechanistic insights were obtained via experimental analysis of transesterification of 2-phenylethyl alcohol (2-PA) with IPA in DMSO by employing various ILs as a potential catalyst.[90] Compared with EimmAc, the catalytic activity of EmimX (X = anionic species) becomes dramatically reduced with weakly basic X^-, such as Cl^-, Br^- and $CF_3CO_2^-$. By contrast, varying cationic species does not have a significant influence on the catalytic activity of ILs as long as Ac^- is employed as the anionic species. This provides experimental evidence that acetate plays a primary catalytic role in transesterification of alcohols and cellulose.

To obtain a detailed and quantitative picture of its reaction pathway, we are currently investingating transesterification of methanol and glucose with IPA using constrained AIMD simulations.

4.4. Activation of Gold Nanocluster Catalysts by ILs

Recently, well-defined gold nanoclusters such as $[Au_{25}(SCH_2CH_2Ph)_{18}]^-$ (denoted as $Au_{25}(SR)_{18}$) have emerged as a promising class of catalysts for the carbon-carbon coupling and other reactions.[91,92] Catalytic effectiveness of such nanoclusters has been demonstrated for many of these reactions. This motivated us to explore the potential catalytic effect of ILs in the nanocluster-catalyzed reactions, in particular Suzuki cross-coupling reaction. It was found that the Suzuki cross-coupling reaction of iodoanisole and phenylboronic acid catalyzed by thiolate-capped Au_{25} cluster supported on TiO_2

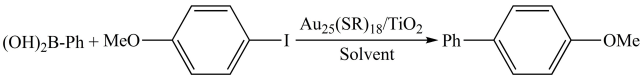

becomes accelerated markedly with the addition of BmimX to the reaction system.[93] While the conversion rate is lower than 5% in common organic solvents, e.g., ethanol and DMF, it increases dramatically to 89–99% with the addition of BmimX. Interestingly, if H2 of $Bmim^+$ is replaced by a methyl group, no catalytic conversion was observed. This suggests that the acidic hydrogen H2 of imidazolium cations (Figure 8b) plays a central role in promoting the cross-coupling reaction. Based on DFT calculations, we have proposed two different mechanisms for oxidative addition of protected gold nanoclusters: (i) adsorption of $Bmim^+$ onto thiolate ligands and (ii) protonation of the protected Au_{25} nanoclusters.[93] The pathway based on the former (Scheme 2) is believed to be the main catalytic mechanism. Specifically, $Bmim^+$ cations adsorb onto thiolate ligands -SR2 and remove fragments of the gold nanocluster, producing active gold sites to catalyze cross-coupling reactions. Compared with common solvents (ethanol and DMF), $Bmim^+$ engender strong interactions with the surface thiolate ligands on the cluster, which is the key for the promotional role of the imidazolium cations.

5. Summary and Outlook

In this account, we have presented a brief overview of our research – large part of it as a collaboration with experimental groups – on spectroscopic and chemical properties of ILs. Key spectral features observed in dielectric absorption, IR and FCS experiments were elucidated and linked to molecular motions. Chemical reactivity/catalytic activity of ILs was illustrated for CO_2 capture and related reactions involving CS_2 as well as

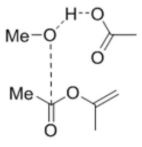

Scheme 1. Activation of methanol by acetate in model transesterification reaction. Adapted from ref. [90] with permission from the Royal Society of Chemistry.

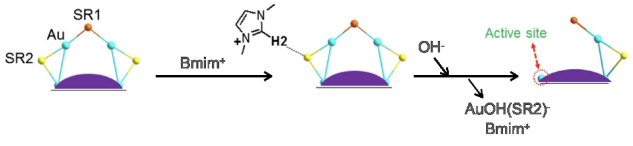

Scheme 2. Activation of the Au_{25} nanocluster promoted by adsorption of imidazolium cations on thiolate ligands. Only the main steps of the proposed mechanism are shown here. SR1 and SR2 are thiolate ligands at two different positions on the surface of Au_{25}. For clarity, their carbon tails are not shown. The purple segment represents the Au_{13} icosahedral core of the Au_{25} nanocluster. Adapted from ref. [93], Copyright (2016), with permission from Elsevier.

transesterification of cellulose and Suzuki cross-coupling reaction catalyzed by gold nanoclusters.

The results highlighted here provide many important insights, and in several cases, novel perspective, on IL spectroscopy, dynamics and reactivity. These include *T*-dependence of dielectric relaxation and dielectric constants, far-IR spectra of Li^+-containing ILs and bimodal photocurrent correlation observed in FCS experiment. Another important discovery was that contrary to a prevalent belief, N-heterocyclic carbene is not likely to be formed in neat imidazolium acetate, implying that the carbene mechanism commonly invoked for many reactions in this IL family may not be in force. Furthermore, predictions of the new concerted mechanism we proposed for CO_2 capture and related reactions are in excellent agreement with experimental results. It would thus be worthwhile, albeit challenging, to scrutinize via AIMD organocatalytic activity of imidazolium acetate in other reactions, such as benzoin condensation,[72–75] and their mechanisms. More broadly, as applications of ionic liquids expand, combined efforts of theory and experiment will be needed more than ever to gain fundamental insights and make new discoveries that will enable and facilitate the advance of IL research and technology.

Acknowledgements

The author is greatly indebted to his collaborators. The list is too long to give here but without their insights and contributions, the IL research presented in this account would not have been possible. Some of the highlighted works were supported in part by the National Science Foundation (Grant Award No. CHE-1223988) and by the U.S. Department of Energy, Office of Basic Sciences, Division of Chemical Sciences, Geosciences, and Biosciences (Grant Award No. DE-SC0019200). The research on IR spectroscopy used resources of the National Energy Research Scientific Computing Center (NERSC), a U.S. Department of Energy Office of Science User Facility located at Lawrence Berkeley National Laboratory, operated under Contract No. DE-AC02-05CH11231 using NERSC awards m3625ERCAP0016009, -ERCAP0017654 and -ERCAP0021569.

Data Availability Statement

The data that support the findings of this study are available from the corresponding author upon reasonable request.

References

[1] T. Welton, *Green Chem.* **2001**, *13*, 225–225.
[2] N. V. Plechkova, K. R. Seddon, *Chem. Soc. Rev.* **2008**, *37*, 123–150.
[3] a) D. R. MacFarlane, N. Tachikawa, M. Forsyth, J. M. Pringle, P. C. Howlett, G. D. Elliott, J. H. Davis, M. Watanabe, P. Simon, C. A. Angell, *Energy Environ. Sci.* **2014**, *7*, 232–250; b) M. Watanabe, M. L. Thomas, S. Zhang, K. Ueno, T. Yasuda, K. Dokko, *Chem. Rev.* **2017**, *117*, 7190–7239.
[4] K. S. Egorova, E. G. Gordeev, V. P. Ananikov, *Chem. Rev.* **2017**, *117*, 7132–7189.
[5] S. Amiril, E. Rahim, S. Syahrullail, *J. Cleaner Prod.* **2017**, *168*, 1571–1589.
[6] V. B. Agbor, N. Cicek, R. Sparling, A. Berlin, D. B. Levin, *Biotechnol. Adv.* **2011**, *29*, 675–685.
[7] See, e.g., *Chem. Rev.* **2017**, *117* (10), special issue on ionic liquids, 6633–7240.
[8] Y. Shim, D. Jeong, S. Manjari, M. Y. Choi, H. J. Kim, *Acc. Chem. Res.* **2007**, *40*, 1130–1137.
[9] J. N. C. Lopes, J. Deschamps, A. A. H. Pádua, *J. Phys. Chem. B* **2004**, *108*, 2038–2047; *J. Phys. Chem. B* **2004**, *108*, 11250.
[10] J. de Andrade, E. S. Böes, H. Stassen, *J. Phys. Chem. B* **2002**, *106*, 13344–13351.
[11] Z. P. Liu, S. P. Huang, W. C. Wang, *J. Phys. Chem. B* **2004**, *108*, 12978–12989.
[12] a) W. L. Jorgensen, D. S. Maxwell, J. Tirado-Rives, *J. Am. Chem. Soc.* **1996**, *118*, 11225–11236; b) G. Kaminski, W. L. Jorgensen, *J. Chem. Soc. Perkin Trans. 2* **1999**, 2365–2375.
[13] a) K. Vanommeslaeghe, E. Hatcher, C. Acharya, S. Kundu, S. Zhong, J. Shim, E. Darian, O. Guvench, P. Lopes, I. Vorobyov, A. D. MacKerell Jr., *J. Comput. Chem.* **2010**, *31*, 671–690; b) K. Vanommeslaeghe, A. D. MacKerell Jr., *J. Chem. Inf. Model.* **2012**, *52*, 3144–3154; c) K. Vanommeslaeghe, E. P. Raman, A. D. MacKerell Jr., *J. Chem. Inf. Model.* **2012**, *52*, 3155–3168.
[14] a) Y. Shim, M. Y. Choi, H. J. Kim, *J. Chem. Phys.* **2005**, *122*, 044510; b) D. Jeong, M. Y. Choi, H. J. Kim, Y. J. Jung, *Phys. Chem. Chem. Phys.* **2010**, *12*, 2001–2010.
[15] T. R. Forster, W. Smith, *The DL_POLY_2.13 Reference Manual*, CCLRC, Daresbury Laboratory. Warrington, **2001**.
[16] M. J. Abraham, T. Murtola, R. Schulz, S. Páll, J. C. Smith, B. Hess, E. Lindahl, *SoftwareX* **2015**, *1–2*, 19–25.
[17] a) A. D. Becke, *Phys. Rev. A* **1988**, *38*, 3098–3100; b) C. Lee, W. Yang, R. G. Parr, *Phys. Rev. B* **1988**, *37*, 785–789.
[18] S. Grimme, J. Antony, S. Ehrlich, H. Krieg, *J. Chem. Phys.* **2010**, *132*, 154104.
[19] T. D. Kühne et al, *J. Chem. Phys.* **2020**, *152*, 194103.
[20] a) C. Schröder, C. Wakai, H. Weingar¨tner, O. Steinhauser, *J. Chem. Phys.* **2007**, *126*, 084511; b) C. Schröder, M. Haberler, O. Steinhauser, *J. Chem. Phys.* **2008**, *128*, 134501; c) C. Schröder, O. Steinhauser, *J. Chem. Phys.* **2009**, *131*, 114504; d) C. Schröder, *J. Chem. Phys.* **2011**, *135*, 024502.
[21] a) Y. Shim, H. J. Kim, *J. Phys. Chem. B* **2008**, *112*, 11028–11038; b) *J. Phys. Chem. B* **2013**, *117*, 11743–11752.
[22] See, e.g., D. A. McQuarrie, *Statistical Mechanics*, HarperCollins, New York, **1976**.
[23] N. R. Dhumal, J. Kiefer, D. Turton, K. Wynne, H. J. Kim, *J. Phys. Chem. B* **2017**, *121*, 4845–4851.

[24] a) K. Fumino, A. Wulf, R. Ludwig, *Angew. Chem. Int. Ed.* **2008**, *47*, 3830–3834; *Angew. Chem.* **2008**, *120*, 3890–3894; b) A. Wulf, K. Fumino, R. Ludwig, P. Taday, *ChemPhysChem* **2010**, *11*, 349–353; c) K. Fumino, S. Reimann, R. Ludwig, *Phys. Chem. Chem. Phys.* **2014**, *16*, 21903–21929.
[25] a) T. Yamada, Y. Tominari, S. Tanaka, M. Mizuno, *J. Phys. Chem. B* **2015**, *119*, 15696–15705; b) *J. Phys. Chem. B* **2017**, *121*, 3121–3129.
[26] D. A. Turton, T. Sonnleitner, A. Ortner, M. Walther, G. Hefter, K. R. Seddon, S. Stana, N. V. Plechkova, R. Buchner, K. Wynne, *Faraday Discuss.* **2012**, *154*, 145–153.
[27] For a recent review and an extensive list of references, see V. H. Paschoal, L. F. O. Faria, M. C. C. Ribeiro, *Chem. Rev.* **2017**, *117*, 7053–7112.
[28] J.-C. Lassègues, J. Grondin, C. Aupetit, P. Johansson, *J. Phys. Chem. A* **2009**, *113*, 305–314.
[29] J. B. Haskins, C. W. Bauschlicher Jr., J. W. Lawson, J. W. J. Phys, *Chem. B* **2015**, *119*, 14705–14719.
[30] F. Yan, K. Mukherjee, M. Maroncelli, H. J. Kim, *J. Phys. Chem. B* **2022**, *126*, 9643–9662.
[31] B. L. Papke, M. A. Ratner, D. F. Shriver, *J. Electrochem. Soc.* **1982**, *129*, 1434–1438.
[32] S. Chang, P. P. Schmidt, M. W. Severson, *J. Phys. Chem.* **1986**, *90*, 1046–1050.
[33] B. Guillot, P. Marteau, J. Obriot, *J. Chem. Phys.* **1990**, *93*, 6148–6164.
[34] a) G. Mathias, M. D. Baer, *J. Chem. Theory Comput.* **2011**, *7*, 2028–2039; b) G. Mathias, S. D. Ivanov, A. Witt, M. D. Baer, D. Marx, *J. Chem. Theory Comput.* **2012**, *8*, 224–234.
[35] N. Molinari, J. P. Mailoa, B. Kozinsky, *J. Phys. Chem. Lett.* **2019**, *10*, 2313–2319.
[36] T. Yamada, M. Mizuno, *ACS Omega* **2021**, *6*, 1709–1717.
[37] T. Köddermann, C. Wertz, A. Heintz, R. Ludwig, *ChemPhysChem* **2006**, *7*, 1944–1949.
[38] a) J. Kiefer, J. Fries, A. Leipertz, *Appl. Spectrosc.* **2007**, *61*, 1306–1311; b) N. R. Dhumal, H. J. Kim, J. Kiefer, *J. Phys. Chem. A* **2009**, *113*, 10397–10404.
[39] S. A. Katsyuba, E. E. Zvereva, A. Vidiš, P. J. Dyson, *J. Phys. Chem. A* **2007**, *111*, 352–370.
[40] a) Y. Jeon, J. Sung, C. Seo, H. Lim, H. Cheong, M. Kang, B. Moon, Y. Ouchi, D. Kim, *J. Phys. Chem. B* **2008**, *112*, 4735–4740; b) S. Cha, M. Ao, W. Sung, B. Moon, B. Ahlström, P. Johansson, Y. Ouchi, D. Kim, *Phys. Chem. Chem. Phys.* **2014**, *16*, 9591–9601.
[41] C. J. Johnson, J. A. Fournier, C. T. Wolke, M. A. Johnson, *J. Chem. Phys.* **2013**, *139*, 224305.
[42] R. Hayes, G. G. Warr, R. Atkin, *Chem. Rev.* **2015**, *115*, 6357–6426 and references therein.
[43] J. Guo, G. A. Baker, P. C. Hillesheim, S. Dai, R. W. Shaw, S. M. Mahurin, *Phys. Chem. Chem. Phys.* **2011**, *13*, 12395–12398.
[44] S. Patra, A. Samanta, *J. Phys. Chem. B* **2012**, *116*, 12275–12283.
[45] E. C. Wu, H. J. Kim, L. A. Peteanu, *J. Phys. Chem. B* **2017**, *121*, 1100–1107.
[46] A. Triolo, O. Russina, V. Arrighi, F. Juranyi, S. Janssen, C. M. Gordon, *J. Chem. Phys.* **2003**, *119*, 8549–8557.
[47] a) O. Yamamuro, T. Yamada, M. Kofu, M. Nakakoshi, M. Nagao, *J. Chem. Phys.* **2011**, *135*, 054508; b) M. Kofu, M. Nagao, T. Ueki, Y. Kitazawa, Y. Nakamura, S. Sawamura, M. Watanabe, O. Yamamuro, *J. Phys. Chem. B* **2013**, *117*, 2773–2781.
[48] a) J. A. Ingram, R. S. Moog, N. Ito, R. Biswas, M. Maroncelli, *J. Phys. Chem. B* **2003**, *107*, 5926–5932; b) S. Arzhantsev, H. Jin, N. Ito, M. Maroncelli, *Chem. Phys. Lett.* **2006**, *417*, 524–529; c) S. Arzhantsev, H. Jin, G. A. Baker, M. Maroncelli, *J. Phys. Chem. B* **2007**, *111*, 4978–4989; d) H. Jin, X. Li, M. Maroncelli, *J. Phys. Chem. B* **2007**, *111*, 13473–13478; e) H. Jin, X. Li, M. Maroncelli, *J. Phys. Chem. B* **2010**, *114*, 11370.
[49] D. Chakrabarty, P. Hazra, A. Chakraborty, D. Seth, N. Sarkar, *Chem. Phys. Lett.* **2003**, *381*, 697–704.
[50] P. K. Chowdhury, M. Halder, L. Sanders, T. Calhoun, J. L. Anderson, D. W. Armstrong, X. Song, J. W. Petrich, *J. Phys. Chem. B* **2004**, *108*, 10245–10255.
[51] a) P. K. Mandal, M. Sarkar, A. Samanta, *J. Phys. Chem. A* **2004**, *108*, 9048–9053; b) A. Samanta, *J. Phys. Chem. B* **2006**, *110*, 13704–13716.
[52] a) H. Shirota, A. M. Funston, J. F. Wishart, E. W. Castner Jr., *J. Chem. Phys.* **2005**, *122*, 184512; b) A. M. Funston, T. A. Fadeeva, J. F. Wishart, E. W. Castner, *J. Phys. Chem. B* **2007**, *111*, 4963–4977.
[53] B. Lang, G. Angulo, E. Vauthey, *J. Phys. Chem. A* **2006**, *110*, 7028–7034.
[54] a) Y. Shim, J. Duan, M. Y. Choi, H. J. Kim, *J. Chem. Phys.* **2003**, *119*, 6411–6414; b) Y. Shim, M. Y. Choi, H. J. Kim, *J. Chem. Phys.* **2005**, *122*, 044511; c) Y. Shim, D. Jeong, M. Y. Choi, H. J. Kim, *J. Chem. Phys.* **2006**, *125*, 061102; d) D. Kim, S.-W. Park, Y. Shim, H. J. Kim, Y. Jung, *J. Chem. Phys.* **2016**, *145*, 044502; e) J. A. L. Willcox, H. Kim, H. J. Kim, *Phys. Chem. Chem. Phys.* **2016**, *18*, 14850–14858.
[55] M. G. Del Pópolo, G. A. Voth, *J. Phys. Chem. B* **2004**, *108*, 1744–1752.
[56] M. N. Kobrak, *J. Chem. Phys.* **2006**, *125*, 064502.
[57] a) Z. Hu, C. J. Margulis, *Proc. Natl. Acad. Sci. USA* **2006**, *103*, 831–836; b) Z. Hu, C. J. Margulis, *Acc. Chem. Res.* **2007**, *40*, 1097–1105; c) J. C. Araque, S. K. Yadav, M. Shadeck, M. Maroncelli, C. J. Margulis, *J. Phys. Chem. B* **2015**, *119*, 7015–7029; d) R. P. Daly, J. C. Araque, C. J. Margulis, *J. Chem. Phys.* **2017**, *147*, 061102.
[58] C. Cadena, Q. Zhao, R. Q. Snurr, E. J. Maginn, *J. Phys. Chem. B* **2006**, *110*, 2821–2832.
[59] a) Z. L. Terranova, S. A. Corcelli, *J. Phys. Chem. B* **2013**, *117*, 15659–15666; b) S. D. Verma, S. A. Corcelli, M. A. Berg, *J. Phys. Chem. Lett.* **2016**, *7*, 504–508.
[60] V. Lesch, A. Heuer, C. Holm, J. Smiatek, *Phys. Chem. Chem. Phys.* **2015**, *17*, 8480–8490.
[61] S. R. Aragón, R. Pecora, *J. Chem. Phys.* **1976**, *64*, 1791–1803.
[62] P. Schwille, J. Korlach, W. W. Webb, *Cytometry* **1999**, *36*, 176–182.
[63] L. O. Hedges, L. Maibaum, D. Chandler, J. P. Garrahan, *J. Chem. Phys.* **2007**, *127*, 211101.
[64] Y. Shim, H. J. Kim, *J. Chem. Phys.* **2006**, *125*, 024507.
[65] C. Dasgupta, A. V. Indrani, S. Ramaswamy, M. K. Phani, *Europhys. Lett.* **1991**, *15*, 307–312.

[66] a) S. C. Glotzer, V. N. Novikov, T. B. Schrøder, *J. Chem. Phys.* **2000**, *112*, 509–512; b) N. Lačevịć, F. W. Starr, T. B. Schrøder, V. N. Novikov, S. C. Glotzer, *Phys. Rev. E* **2002**, *66*, 030101; c) N. Lačevịć, F. W. Starr, T. B. Schrøder, S. C. Glotzer, *J. Chem. Phys.* **2003**, *119*, 7372–7387.
[67] a) L. Berthier, *Phys. Rev. E* **2004**, *69*, 020201; b) C. Toninelli, M. Wyart, L. Berthier, G. Biroli, J.-P. Bouchaud, *Phys. Rev. E* **2005**, *71*, 041505.
[68] S. Karmakar, C. Dasgupta, S. Sastry, *Proc. Natl. Acad. Sci. USA* **2009**, *106*, 3675–3679.
[69] K. Kim, S. Saito, *J. Chem. Phys.* **2013**, *138*, 12A506.
[70] J. Liu, J. A. L. Willcox, H. J. Kim, *J. Chem. Phys.* **2018**, *148*, 193830.
[71] H. Rodríguez, G. Gurau, J. D. Holbrey, R. D. Rogers, *Chem. Commun.* **2011**, *47*, 3222–3224.
[72] Z. Kelemen, O. Hollóczki, J. Nagy, L. Nyulászi, *Org. Biomol. Chem.* **2011**, *9*, 5362–5364.
[73] D. J. Liu, Y. Zhang, E. Y.-X. Chen, *Green Chem.* **2012**, *14*, 2738–2746.
[74] I. Chiarotto, M. Feroci, A. Inesi, *New J. Chem.* **2017**, *41*, 7840–7843.
[75] N. M. A. N. Daud, E. Bakis, J. Hallett, C. C. Weber, T. Welton, *Chem. Commun.* **2017**, *53*, 11154–11156.
[76] E. J. Maginn, *Quarterly Technical Report to DOE* **2005**.
[77] G. Gurau, H. Rodríguez, S. P. Kelley, P. Janiczek, R. S. Kalb, R. D. Rogers, *Angew. Chem. Int. Ed.* **2011**, *50*, 12024–12026.
[78] a) M. Besnard, M. I. Cabaço, F. V. Chávez, N. Pinaud, P. J. Sebastião, J. A. P. Coutinho, Y. Danten, *Chem. Commun.* **2012**, *48*, 1245–1247; b) M. I. Cabaço, M. Besnard, Y. Danten, J. A. P. Coutinho, *J. Phys. Chem. A* **2012**, *116*, 1605–1620; c) M. Besnard, M. I. Cabaço, F. V. Chávez, N. Pinaud, P. J. Sebastião, J. A. P. Coutinho, J. Mascetti, Y. Danten, *J. Phys. Chem. A* **2012**, *116*, 4890–4901.
[79] a) W. Shi, C. R. Meyers, D. R. Luebke, J. A. Steckel, D. C. Sorescu, *J. Phys. Chem. B* **2012**, *116*, 283–295; b) J. X. Mao, J. A. Steckel, F. Yan, N. R. Dhumal, D. R. Luebke, H. J. Kim, K. Damodaran, *Phys. Chem. Chem. Phys.* **2016**, *18*, 1911–1917.
[80] O. Hollóczki, D. S. Firaha, J. Friedrich, M. Brehm, R. Cybik, M. Wild, A. Stark, B. Kirchner, *J. Phys. Chem. B* **2013**, *117*, 5898–5907.
[81] F. Yan, N. R. Dhumal, H. J. Kim, *Phys. Chem. Chem. Phys.* **2017**, *19*, 1361–1368.
[82] a) M. I. Cabaço, M. Besnard, F. V. Chávez, N. Pinaud, P. J. Sebastião, J. A. P. Coutinho, J. Mascetti, Y. Danten, *Chem. Commun.* **2013**, *49*, 11083–11085; b) M. I. Cabaço, M. Besnard, F. V. Chávez, N. Pinaud, P. J. Sebastião, J. A. P. Coutinho, Y. Danten, *J. Chem. Phys.* **2014**, *140*, 244307; c) Y. Danten, M. I. Cabaco¸, J. A. P. Coutinho, N. Pinaud, M. Besnard, *J. Phys. Chem. B* **2016**, *120*, 5243–5254.
[83] F. Yan, R. Kakuchi, K. Takahashi, H. J. Kim, *Phys. Chem. Chem. Phys.* **2018**, *20*, 19339–19349.
[84] R. P. Swatloski, S. K. Spear, J. D. Holbrey, R. D. Rogers, *J. Am. Chem. Soc.* **2002**, *124*, 4974–4975.
[85] A. Pinkert, K. N. Marsh, S. Pang, M. P. Staiger, *Chem. Rev.* **2009**, *109*, 6712–6728.
[86] H. Tadesse, R. Luque, *Energy Environ. Sci.* **2011**, *4*, 3913–3929.
[87] M. Gericke, P. Fardim, T. Heinze, *Molecules* **2012**, *17*, 7458–7502.
[88] a) T. Endo, S. Hosomi, S. Fujii, K. Ninomiya, K. Takahashi, *J. Phys. Chem. Lett.* **2016**, *7*, 5156–5161; b) T. Endo, E. M. Aung, S. Fujii, S. Hosomi, M. Kimizu, K. Ninomiya, K. Takahashi, *Carbohydr. Polym.* **2017**, *176*, 365–373; c) K. Kuroda, H. Satria, K. Miyamura, K. Ninomiya, K. Takahashi, *J. Am. Chem. Soc.* **2017**, *139*, 16052–16055.
[89] R. Kakuchi, M. Yamaguchi, T. Endo, Y. Shibata, K. Ninomiya, T. Ikai, K. Maeda, K. Takahashi, *RSC Adv.* **2015**, *5*, 72071–72074.
[90] R. Kakuchi, R. Ito, S. Nomura, H. Abroshan, K. Ninomiya, T. Ikai, K. Maeda, H. J. Kim, K. Takahashi, *RSC Adv.* **2017**, *7*, 9423–9430; **2017**, *7*, 13876.
[91] a) G. Li, R. Jin, *Acc. Chem. Res.* **2013**, *46*, 1749–1758; b) G. Li, D. Jiang, C. Liu, C. Yu, R. Jin, *J. Catal.* **2013**, *306*, 177–183; c) Z. Wu, D. Jiang, A. K. P. Mann, D. R. Mullins, Z. Qiao, L. F. Allard, C. Zeng, R. Jin, S. H. Overbury, *J. Am. Chem. Soc.* **2014**, *136*, 6111–6122; d) G. Li, R. Jin, *J. Am. Chem. Soc.* **2014**, *136*, 11347–11354.
[92] S. Yamazoe, K. Koyasu, T. Tsukuda, *Acc. Chem. Res.* **2014**, *47*, 816–824.
[93] H. Abroshan, G. Li, H. J. Kim, R. Jin, *J. Catal.* **2016**, *337*, 72–79.

Manuscript received: February 27, 2023
Revised manuscript received: April 18, 2023
Version of record online: May 11, 2023

